Draft version April 26, 2015
Preprint typeset using LaTeX style emulateapj v. 01/23/15

SUPERMASSIVE BLACK HOLES AND HOST BULGES AFFAIRS – II. THE RED AND THE BLUE SEQUENCES IN THE MASS – MASS DIAGRAM.

G. A. D. Savorgnan and A. W. Graham
Centre for Astrophysics and Supercomputing, Swinburne University of Technology, Hawthorn, Victoria 3122, Australia.

A. Marconi
?

E. Sani
European Southern Observatory, Alonso de Cordova, Vitacura 3107, Santiago, Chile.

and

L.K. Hunt
?

Draft version April 26, 2015

ABSTRACT

We present the latest scaling relations between black hole mass, $M_{\rm BH}$, and spheroid luminosity, $L_{\rm sph}$, spheroid stellar mass, $M_{*,\rm sph}$, and galaxy luminosity, $L_{\rm gal}$, built upon an unprecedented high-quality data set (provided here in a ready-to-use table). Our sample, the largest ever used, counts 66 local galaxies with a dynamical measurement of $M_{\rm BH}$. Luminosities come from high signal-to-noise 3.6 μm *Spitzer* satellite imagery, which is minimally affected by dust and star formation. These luminosities were derived from our state-of-the-art multicomponent galaxy decompositions, that take into account bulges, disks, bars, spiral arms, rings, haloes, extended or unresolved nuclear sources and partially depleted cores, and that – for the first time – were checked to be consistent with the galaxy kinematics. Previous studies used galaxy samples that were overwhelmingly dominated by high-mass, early-type objects. Instead, our sample includes 17 spiral galaxies, half of which have $M_{\rm BH} < 10^7$ M$_\odot$, and allows us to investigate the poorly studied low-mass end of the correlations. We provide updated linear regressions (symmetrical, to be compared with theoretical expectations, and non-symmetrical, to be used to predict black hole masses) for Sérsic/core-Sérsic galaxies and for different morphological types (E/S0, Sp). The bulges of early-type (E/S0) galaxies follow $M_{\rm BH} \propto M_{*,\rm sph}^{1.0\pm0.1}$, as expected from a dry-merging formation scenario, and define a tight *red sequence* with intrinsic scatter $\epsilon = 0.43 \pm 0.06$ dex. On the other hand, the bulges of late-type (Sp) galaxies define a much steeper *blue sequence*, with $M_{\rm BH} \propto M_{*,\rm sph}^{3.0\pm1.3}$, indicating that gas-rich processes feed the black hole three times more efficiently than the host bulge. Disproving some previous claims, we also conclude that: 1) Sérsic and core-Sérsic galaxies do not define two distinct sequences; 2) bulges with Sérsic index $n_{\rm sph} < 2$, argued by some to be pseudo-bulges, are not offset to lower $M_{\rm BH}$ from the correlation defined by bulges with $n_{\rm sph} > 2$; 3) $L_{\rm sph}$ and $L_{\rm gal}$ correlate equally well with $M_{\rm BH}$, in terms of intrinsic scatter, only for early-type galaxies.

Subject headings: keywords

1. INTRODUCTION

More than two and a half decades ago, Dressler (1989) foresaw a "rough scaling of black hole mass with the mass of the spheroidal component", as suggested by the sequence of five galaxies (M87, M104, M31, M32 and the Milky Way). His "rough scaling" was a premature version of the nowadays popular correlation between black hole mass, $M_{\rm BH}$, and host spheroid luminosity, $L_{\rm sph}$, and also host spheroid mass, $M_{\rm sph}$ (Yee 1992; Kormendy & Richstone 1995; Magorrian et al. 1998; Marconi & Hunt 2003; Häring & Rix 2004). These early studies were dominated by high-mass, early-type galaxies, for which they reported a quasi-linear $M_{\rm BH} - M_{\rm sph}$ relation, consistent with a dry-merging formation scenario. Subsequent studies of the $M_{\rm BH} - L_{\rm sph}$ and $M_{\rm BH} - M_{\rm sph}$ diagrams (Ferrarese & Ford 2005; Lauer et al. 2007a; Graham 2007, 2008; Gültekin et al. 2009; Sani et al. 2011; Beifiori et al. 2012; Erwin & Gadotti 2012; Vika et al. 2012; van den Bosch et al. 2012; McConnell & Ma 2013; Kormendy & Ho 2013; Rusli et al. 2013a; see Graham 2015b for an extensive review about the early discovery and successive improvements of these correlations) used similar galaxy samples, which remained dominated by high-mass, early-type objects having $M_{\rm BH} \gtrsim 0.5 \times 10^8$ M$_\odot$, and recovered a near-linear relation. However, the consensus about a linear $M_{\rm BH} - M_{\rm sph}$ correlation was not unanimous. Some studies reported a slope steeper than one, or noticed that low-mass spheroids were downwards offset from the relation traced by their high-mass counterparts (Laor 1998; Wandel 1999; Laor 2001; Ryan et al. 2007). Recently,

gsavorgn@astro.swin.edu.au

Läsker et al. (2014a,b) derived 2.2 μm bulge luminosities for 35 galaxies (among which only 4 were classified as spiral galaxies), and reported a slope below unity for their $M_{\rm BH} - M_{\rm sph}$ relation. They also claimed that the black hole mass correlates equally well with the total galaxy luminosity as it does with the bulge luminosity.

The $M_{\rm BH} - L_{\rm sph}$ relation can be predicted from other two correlations involving the bulge velocity dispersion, σ. The first of these two is the $M_{\rm BH} - \sigma$ relation (Ferrarese & Merritt 2000; Gebhardt et al. 2000), which can be described by a single power-law ($M_{\rm BH} \propto \sigma^5$) over the range in velocity dispersion $70 - 350$ km s^{-1} (e.g. Graham et al. 2011; McConnell et al. 2011; Graham & Scott 2013). The second is the $L_{\rm sph} - \sigma$ relation, which has long been known to be a "double power-law", being $L_{\rm sph} \propto \sigma^5$ at the luminous end (Schechter 1980; Malumuth & Kirshner 1981; von der Linden et al. 2007; Liu et al. 2008), and $L_{\rm sph} \propto \sigma^2$ at intermediate and faint luminosities (Davies et al. 1983; Held et al. 1992; Matković & Guzmán 2005; de Rijcke et al. 2005; Balcells et al. 2007; Chilingarian et al. 2008; Forbes et al. 2008; Cody et al. 2009; Tortora et al. 2009; Kourkchi et al. 2012). The change in slope of the $L_{\rm sph} - \sigma$ relation occurs at $M_B \approx -20.5$ mag, corresponding to $\sigma \approx 200$ km s^{-1}. That is, the $M_{\rm BH} - L_{\rm sph}$ relation should be better described by a "broken", rather than a single, power-law, having $M_{\rm BH} \propto L_{\rm sph}^{2.5}$ at the low-luminosity end, and $M_{\rm BH} \propto L_{\rm sph}^{1}$ at the high-luminosity end. Due to the scatter in the $M_{\rm BH} - L_{\rm sph}$ (or $M_{\rm BH} - M_{\rm sph}$) diagram, studies that have not sufficiently probed below $M_{\rm BH} \approx 10^7$ M$_\odot$ can easily miss the change in slope occuring at $M_{\rm BH} \approx 10^{(8\pm1)}$ M$_\odot$, and erroneously recover a single log-linear relation.

When Graham (2012) pointed out this overlooked inconsistency, he identified two different populations of galaxies, namely the core-Sérsic (Graham et al. 2003; Trujillo et al. 2004) and Sérsic spheroids[1], and attributed the change in slope (from log-quadratic to log-linear) to their different formation mechanisms. In this scenario, core-Sérsic spheroids are built in additive dry merger events, where the black hole and the bulge grow at the same pace, increasing their mass in lock steps ($M_{\rm BH} \propto L_{\rm sph}^{1}$), whereas Sérsic spheroids originate from gas-rich processes, in which the mass of the black hole increases more rapidly than the mass of its host spheroid ($M_{\rm BH} \propto L_{\rm sph}^{2.5}$). Graham & Scott (2013, hereafter GS13) and Scott et al. (2013, hereafter S+13) presented double power-law linear regressions for Sérsic/core-Sérsic spheroids in the $M_{\rm BH} - L_{\rm sph}$ and $M_{\rm BH} - M_{*,\rm sph}$ (spheroid stellar mass) diagrams, respectively, probing down to $M_{\rm BH} \approx 10^6$ M$_\odot$. To obtain their dust-corrected *bulge* magnitudes, they did not perform bulge/disc decompositions, but instead they converted $B-$band and K_S-band observed, total *galaxy* magnitudes using a mean statistical correction based on each object's morphological type and disc inclination[2]. However, this mean statistical correction was obtained from the results of non-modern bulge/disk decompositions, which did not include extra components. It should also be noted that ∼80% of their core-Sérsic spheroids were morphologically classified as elliptical galaxies, and ∼80% of their Sérsic spheroids were morphologically classified as bulges of disk galaxies (lenticulars and spirals).

Several recent papers (Jiang et al. 2011, 2013; Mathur et al. 2012; Reines et al. 2013) claimed an offset at the low-mass end of the $M_{\rm BH} - M_{*,\rm sph}$ diagram, such that the black hole mass is lower than expected from the near-linear correlation traced by the high-mass, early-type spheroids. However, Graham & Scott (2015) showed that the low-mass spheroids ($10^{8.5} \lesssim M_{*,\rm sph}/{\rm M}_\odot \lesssim 10^{10.5}$) are not somehow randomly offset from the high-mass, near-linear correlation, but lie on the two times steeper relation traced by the Sérsic spheroids. **AL: would you like to add a sentence here, mentioning your forthcoming paper with ewan?**

Here we investigate substructure in the $M_{\rm BH} - L_{\rm sph}$ and $M_{\rm BH} - M_{*,\rm sph}$ diagrams using state-of-the-art galaxy decompositions (Savorgnan & Graham *in preparation*, hereafter *Paper I*) for the largest sample of galaxies with directly measured black hole masses. Our galaxies are large and nearby, which allows us to perform accurate multi-component decompositions (instead of simple bulge/disk decompositions) without incurring in significant parameter degeneracies. Our decompositions were obtained from 3.6 μm *Spitzer* satellite imagery, which is an excellent proxy for the stellar mass, superior to the $K-$band (Sheth et al. 2010 and references therein). Nine of our galaxies have $M_{\rm BH} \lesssim 10^7$ M$_\odot$, which allows us to accurately constrain the slope of the correlation at the low-mass end. In addition to this, our galaxy sample includes 17 spiral galaxies, representing a notable improvement over the past studies dominated by early-type systems. In a forthcoming paper, we will explore the relation between black hole mass and bulge dynamical mass, $M_{\rm dyn,sph} \propto R_{\rm e}\sigma^2$, and address the issue of a black hole fundamental plane. This paper is structured as follows...

2. DATA

Our galaxy sample (see Table 1) consists of 66 objects for which a dynamical measurement of the black hole mass had been reported in the literature (by GS13 or Rusli et al. 2013b) at the time we started this project, and for which we were able to obtain useful bulge parameters from 3.6 μm *Spitzer* satellite imagery. Bulge magnitudes were derived from our state-of-the-art galaxy decompositions, which take into account bulges, disks, spiral arms, bars, rings, haloes, extended or unresolved nuclear sources and partially depleted cores. Kinematical information (Emsellem et al. 2011; Scott et al. 2014; Arnold et al. 2014) was used to confirm the presence of rotationally supported components in most early-type galaxies, and to identify their extent (intermediate-scale disks, that are fully embedded in the bulge, or large-scale disks, that encase the bulge and dominate the light

[1] Core-Sérsic spheroids have partially depleted cores relative to their outer Sérsic light profile, whereas Sérsic spheroids have no central deficit of stars. While core-Sérsic spheroids are also "core galaxies", as given by the Nuker definition (Lauer et al. 2007b), it should be noted that ∼20% of "core galaxies" are not core-Sérsic spheroids (Dullo & Graham 2014, their Appendix A.2), i.e. do not have depleted cores. The change in slope of the $L_{\rm sph} - \sigma$ relation corresponds to the division between core-Sérsic and Sérsic spheroids (e.g. Graham & Guzmán 2003).

[2] While this resulted in individual bulge magnitudes not being exactly correct, their large sample size allowed them to obtain a reasonably ensemble average correction.

at large radii). *Paper I* will present the dataset used here to investigate the $M_{\rm BH} - L_{\rm sph}$ and $M_{\rm BH} - M_{*,\rm sph}$ diagrams, give details about the data reduction process and the sophisticated galaxy modelling technique that we developed, discuss how we estimated the uncertainties[3] on the bulge magnitudes, and illustrate the individual 66 galaxy decompositions.

Bulge luminosities[4] were first converted into stellar masses using a constant 3.6 μm mass-to-light ratio, $\Gamma_{3.6} = 0.6$ (Meidt et al. 2014). We then explored a more sophisticated way to compute mass-to-light ratios, using the color-$\Gamma_{3.6}$ relation published by Meidt et al. (2014, their equation 4), which allows one to estimate $\Gamma_{3.6}$ of a galaxy from its $[3.6]-[4.5]$ color. Individual $[3.6]-[4.5]$ colors[5] were taken from Peletier et al. (2012, column 8 of their Table 1) when available for our galaxies, or were estimated from the bulge stellar velocity dispersion, σ, using the color-σ relation presented by Peletier et al. (2012, their Figure 6). We found that the range in $[3.6]-[4.5]$ color is small (0.06 mag), and thus the range in $\Gamma_{3.6}$ is also small (0.04). After checking that using a single $\Gamma_{3.6} = 0.6$, independent of $[3.6]-[4.5]$ color, does not significantly affect the results of our analysis, we decided to use individual, color-dependent mass-to-light ratios.

The Sérsic/core-Sérsic classification presented in this work comes from the compilation of Savorgnan & Graham (2014), who identified partially depleted cores according to the same criteria used by GS13. When no high-resolution image analysis was available from the literature, they inferred the presence of a partially depleted core based on the stellar velocity dispersion: a galaxy is classified as core-Sérsic if $\sigma > 270$ km s^{-1}, or as Sérsic if $\sigma < 166$ km s^{-1}.

For each galaxy, the total luminosity (or galaxy luminosity, $L_{\rm gal}$) is the sum of the luminosities of all its subcomponents. Due to the complexity of their modelling, four galaxies (see Table 1, column 7) had their galaxy luminosities underestimated[6], which are given here as lower limits. Following GS13, we assumed a constant uncertainty of 0.25 mag for all galaxy magnitudes.

3. ANALYSIS

We performed a linear regression analysis of the $M_{\rm BH} - L_{\rm sph}$, $M_{\rm BH} - M_{*,\rm sph}$ and $M_{\rm BH} - L_{\rm gal}$ diagrams using the BCES code from Akritas & Bershady (1996). We also repeated the analysis with the FITEXY routine (Press et al. 1992), modified by Tremaine et al. (2002), and the Bayesian estimator `linmix_err` (Kelly 2007). Although all these three linear regression routines account for the intrinsic scatter, only the last two allow

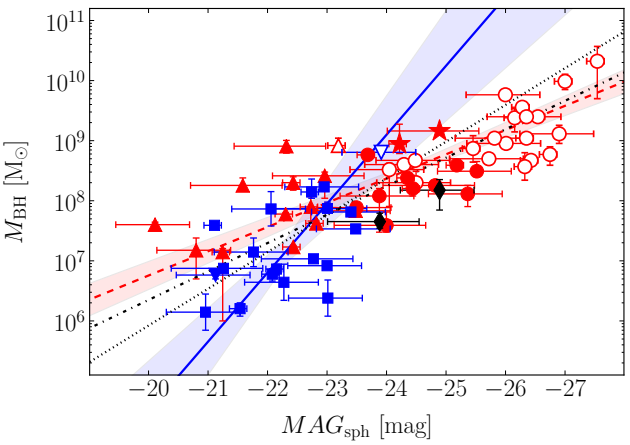

FIG. 1.— Black hole mass against 3.6 μm spheroid absolute magnitude. Symbols are coded according to the galaxy morphological type: red circle = elliptical, red star = elliptical/lenticular, red upward triangle = lenticular, blue downward triangle = lenticular/spiral, blue square = spiral, black diamond = merger. Empty symbols represent core-Sérsic spheroids, whereas filled symbols are used for Sérsic spheroids. The red dashed line indicates the BCES bisector linear regression for early-type galaxies (ellipticals+lenticulars), with the red shaded area denoting its 1σ uncertainty. The blue solid line shows the BCES bisector linear regression for spiral galaxies, with the blue shaded area denoting its 1σ uncertainty. The black dashed-dotted and dotted lines represent the BCES bisector linear regressions for core-Sérsic and Sérsic spheroids, respectively.

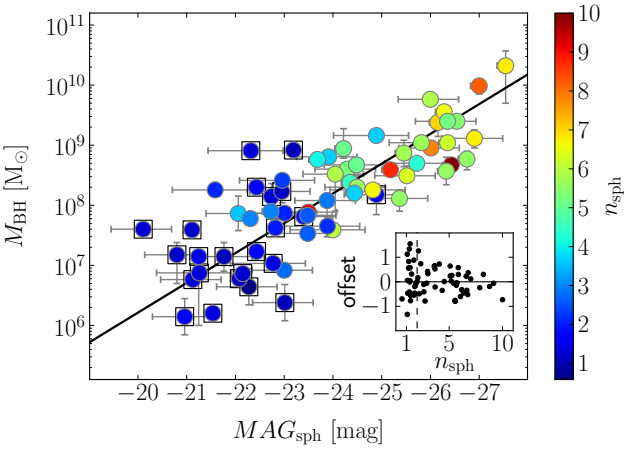

FIG. 2.— Black hole mass against 3.6 μm spheroid absolute magnitude. Symbols are color coded according to the spheroid Sérsic index $n_{\rm sph}$. Bulges with $n_{\rm sph} < 2$, claimed by some to be pseudobulges, are marked with an empty square. The black solid line shows the BCES bisector linear regression for spheroids with $n_{\rm sph} \geq 2$. The inset displays, for all spheroids, the vertical offset from the correlation defined by spheroids with $n_{\rm sph} \geq 2$ only versus the spheroid Sérsic index. The vertical dashed line corresponds to $n_{\rm sph} = 2$. Bulges with $n_{\rm sph} < 2$ are not randomly offset to lower black hole masses from the correlation traced by bulges with $n_{\rm sph} \geq 2$.

[3] By comparing, for our galaxies, the measurements of the bulge magnitude obtained by different authors with those obtained by us, we estimated the uncertainties on the bulge magnitudes with a method that takes into account systematic errors. Systematic errors include incorrect sky subtraction, inaccurate masking of contaminating sources, imprecise description of the PSF, erroneous choice of model components (for example, when failing to identify a galaxy subcomponent and thus omitting it in the model, or when describing a galaxy sub-component with an inadequate function), the radial extent of the surface brightness profile and its sampling. These factors are not included in popular 2D fitting codes which report only the random errors associated with their fitted parameters. In fact, when performing multi-component decomposition of high signal-to-noise images of nearby – therefore well spatially resolved – galaxies, errors are dominated by systematics rather than Poisson noise.

[4] Absolute luminosities were calculated assuming a 3.6 μm solar absolute magnitude of 3.25 mag (Sani et al. 2011).

[5] These are integrated $[3.6]-[4.5]$ colors, measured in a circular aperture within one galaxy's effective radius.

[6] These four cases will be discussed in *Paper I*.

TABLE 1

Galaxy sample. *Column (1):* Galaxy name. *Column (2):* Morphological type (E=elliptical, S0(B)=(barred) lenticular, Sp(B)=(barred) spiral, merger=merger). *Column (3):* Presence of a partially depleted core. The question mark is used when the classification has come from the velocity dispersion criteria mentioned in Section 2. *Column (4):* Distance. *Column (5):* Black hole mass. *Column (6):* Absolute 3.6 μm bulge magnitude. *Column (7):* Absolute 3.6 μm galaxy magnitude. The four galaxy magnitudes marked with a * are upper limits. *Column (8):* [3.6] − [4.5] colour. *Column (9):* Bulge stellar mass.

Galaxy	**Type**	**Core**	**Distance** [Mpc]	$M_{\mathbf{BH}}$ [10^8 $M_\odot$]	$MAG_{\mathbf{sph}}$ [mag]	$MAG_{\mathbf{gal}}$ [mag]	**[3.6] − [4.5]** [mag]	$M_{*,\mathbf{sph}}$ [10^{10} $M_\odot$]
(1)	(2)	(3)	(4)	(5)	(6)	(7)	(8)	(9)
IC 1459	E	yes	28.4	24^{+10}_{-10}	$-26.15^{+0.18}_{-0.11}$	-26.15 ± 0.15	−0.12	27^{+30}_{-23}
IC 2560	SpB	no?	40.7	$0.044^{+0.044}_{-0.022}$	$-22.27^{+0.66}_{-0.58}$	-24.76 ± 0.08	−0.08	$1.0^{+1.8}_{-0.6}$
IC 4296	E	yes?	40.7	11^{+2}_{-2}	$-26.35^{+0.18}_{-0.11}$	-26.35 ± 0.10	−0.12	31^{+34}_{-26}
M104	S0/Sp	yes	9.5	$6.4^{+0.4}_{-0.4}$	$-23.91^{+0.66}_{-0.58}$	-25.21 ± 0.06	−0.12	$3.4^{+5.8}_{-1.9}$
M105	E	yes	10.3	4^{+1}_{-1}	$-24.29^{+0.66}_{-0.58}$	-24.29 ± 0.27	−0.10	$5.6^{+9.5}_{-3.0}$
M106	SpB	no	7.2	$0.39^{+0.01}_{-0.01}$	$-21.11^{+0.18}_{-0.11}$	-24.04 ± 0.17	−0.08	$0.37^{+0.41}_{-0.31}$
M31	SpB	no	0.7	$1.4^{+0.9}_{-0.3}$	$-22.74^{+0.18}_{-0.11}$	-24.67 ± 0.02	−0.09	$1.5^{+1.6}_{-1.3}$
M49	E	yes	17.1	25^{+3}_{-1}	$-26.54^{+0.18}_{-0.11}$	-26.54 ± 0.11	−0.12	39^{+43}_{-33}
M59	E	no	17.8	$3.9^{+0.4}_{-0.4}$	$-25.18^{+0.18}_{-0.11}$	-25.27 ± 0.02	−0.09	14^{+15}_{-11}
M64	Sp	no?	7.3	$0.016^{+0.004}_{-0.004}$	$-21.54^{+0.18}_{-0.11}$	-24.24 ± 0.06	−0.06	$0.64^{+0.71}_{-0.55}$
M81	SpB	no	3.8	$0.74^{+0.21}_{-0.11}$	$-23.01^{+0.88}_{-0.66}$	-24.43 ± 0.30	−0.09	$1.9^{+3.6}_{-0.9}$
M84	E	yes	17.9	$9.0^{+0.9}_{-0.8}$	$-26.01^{+0.66}_{-0.58}$	-26.01 ± 0.02	−0.10	28^{+47}_{-15}
M87	E	yes	15.6	$58.0^{+3.5}_{-3.5}$	$-26.00^{+0.66}_{-0.58}$	-26.00 ± 0.12	−0.11	26^{+44}_{-14}
M89	E	yes	14.9	$4.7^{+0.5}_{-0.5}$	$-24.48^{+0.66}_{-0.58}$	-24.74 ± 0.10	−0.11	$6.3^{+10.7}_{-3.4}$
M94	SpB	no?	4.4	$0.060^{+0.014}_{-0.014}$	$-22.08^{+0.18}_{-0.11}$	-23.36 ± 0.08 *	−0.07	$1.00^{+1.11}_{-0.85}$
M96	SpB	no	10.1	$0.073^{+0.015}_{-0.015}$	$-22.15^{+0.18}_{-0.11}$	-24.20 ± 0.27	−0.08	$0.97^{+1.08}_{-0.83}$
NGC 0524	S0	yes	23.3	$8.3^{+2.7}_{-1.3}$	$-23.19^{+0.18}_{-0.11}$	-24.92 ± 0.05	−0.09	$2.2^{+2.5}_{-1.9}$
NGC 0821	E	no	23.4	$0.39^{+0.26}_{-0.09}$	$-24.00^{+0.88}_{-0.66}$	-24.26 ± 0.01	−0.09	$4.7^{+8.7}_{-2.1}$
NGC 1023	S0B	no	11.1	$0.42^{+0.04}_{-0.04}$	$-22.82^{+0.18}_{-0.11}$	-24.20 ± 0.02	−0.10	$1.5^{+1.7}_{-1.3}$
NGC 1300	SpB	no	20.7	$0.73^{+0.69}_{-0.35}$	$-22.06^{+0.66}_{-0.58}$	-24.16 ± 0.00	−0.10	$0.70^{+1.19}_{-0.38}$
NGC 1316	merger	no	18.6	$1.50^{+0.75}_{-0.80}$	$-24.89^{+0.66}_{-0.58}$	-26.48 ± 0.05	−0.10	$9.5^{+16.2}_{-5.2}$
NGC 1332	E/S0	no	22.3	14^{+2}_{-2}	$-24.89^{+0.88}_{-0.66}$	-24.95 ± 0.03	−0.12	$8.2^{+15.0}_{-3.6}$
NGC 1374	E	no?	19.2	$5.8^{+0.5}_{-0.5}$	$-23.68^{+0.18}_{-0.11}$	-23.70 ± 0.08	−0.09	$3.6^{+4.0}_{-3.0}$
NGC 1399	E	yes	19.4	$4.7^{+0.6}_{-0.6}$	$-26.43^{+0.18}_{-0.11}$	-26.46 ± 0.04	−0.12	33^{+37}_{-28}
NGC 2273	SpB	no	28.5	$0.083^{+0.004}_{-0.004}$	$-23.00^{+0.66}_{-0.58}$	-24.21 ± 0.15	−0.08	$2.0^{+3.4}_{-1.1}$
NGC 2549	S0B	no	12.3	$0.14^{+0.02}_{-0.13}$	$-21.25^{+0.18}_{-0.11}$	-22.60 ± 0.02	−0.10	$0.35^{+0.39}_{-0.30}$
NGC 2778	S0B	no	22.3	$0.15^{+0.09}_{-0.10}$	$-20.80^{+0.66}_{-0.58}$	-22.44 ± 0.07	−0.09	$0.25^{+0.43}_{-0.14}$
NGC 2787	S0B	no	7.3	$0.40^{+0.04}_{-0.05}$	$-20.11^{+0.66}_{-0.58}$	-22.28 ± 0.06	−0.10	$0.12^{+0.20}_{-0.07}$
NGC 2974	SpB	no	20.9	$1.7^{+0.2}_{-0.2}$	$-22.95^{+0.66}_{-0.58}$	-24.16 ± 0.04	−0.09	$1.8^{+3.1}_{-1.0}$
NGC 3079	SpB	no?	20.7	$0.024^{+0.024}_{-0.012}$	$-23.01^{+0.66}_{-0.58}$	-24.45 ± 0.04 *	−0.07	$2.4^{+4.0}_{-1.3}$
NGC 3091	E	yes	51.2	36^{+1}_{-2}	$-26.28^{+0.18}_{-0.11}$	-26.28 ± 0.09	−0.12	30^{+34}_{-26}
NGC 3115	E/S0	no	9.4	$8.8^{+10.0}_{-2.7}$	$-24.22^{+0.18}_{-0.11}$	-24.40 ± 0.02	−0.11	$4.9^{+5.4}_{-4.1}$
NGC 3227	SpB	no	20.3	$0.14^{+0.10}_{-0.06}$	$-21.76^{+0.66}_{-0.58}$	-24.26 ± 0.10	−0.08	$0.67^{+1.15}_{-0.37}$
NGC 3245	S0B	no	20.3	$2.0^{+0.5}_{-0.5}$	$-22.43^{+0.18}_{-0.11}$	-23.88 ± 0.03	−0.10	$1.0^{+1.1}_{-0.9}$
NGC 3377	E	no	10.9	$0.77^{+0.04}_{-0.06}$	$-23.49^{+0.66}_{-0.58}$	-23.57 ± 0.06	−0.06	$4.0^{+6.8}_{-2.2}$
NGC 3384	S0B	no	11.3	$0.17^{+0.01}_{-0.02}$	$-22.43^{+0.18}_{-0.11}$	-23.74 ± 0.01	−0.08	$1.2^{+1.3}_{-1.0}$
NGC 3393	SpB	no	55.2	$0.34^{+0.02}_{-0.02}$	$-23.48^{+0.66}_{-0.58}$	-25.29 ± 0.10	−0.10	$2.8^{+4.7}_{-1.5}$
NGC 3414	E	no	24.5	$2.4^{+0.3}_{-0.3}$	$-24.35^{+0.18}_{-0.11}$	-24.42 ± 0.02	−0.09	$6.5^{+7.2}_{-5.5}$
NGC 3489	S0/SpB	no	11.7	$0.058^{+0.008}_{-0.008}$	$-21.13^{+0.66}_{-0.58}$	-23.07 ± 0.05	−0.06	$0.42^{+0.72}_{-0.23}$
NGC 3585	E	no	19.5	$3.1^{+1.4}_{-0.6}$	$-25.52^{+0.66}_{-0.58}$	-25.55 ± 0.03	−0.10	18^{+30}_{-10}
NGC 3607	E	no	22.2	$1.3^{+0.5}_{-0.5}$	$-25.36^{+0.66}_{-0.58}$	-25.45 ± 0.11	−0.10	15^{+25}_{-8}
NGC 3608	E	yes	22.3	$2.0^{+1.1}_{-0.6}$	$-24.50^{+0.66}_{-0.58}$	-24.50 ± 0.15	−0.08	$7.8^{+13.4}_{-4.3}$
NGC 3842	E	yes	98.4	97^{+30}_{-26}	$-27.00^{+0.18}_{-0.11}$	-27.04 ± 0.06	−0.11	61^{+68}_{-52}
NGC 3998	S0B	no	13.7	$8.1^{+2.0}_{-1.9}$	$-22.32^{+0.88}_{-0.66}$	-23.53 ± 0.01	−0.12	$0.78^{+1.43}_{-0.35}$
NGC 4026	S0B	no	13.2	$1.8^{+0.6}_{-0.3}$	$-21.58^{+0.88}_{-0.66}$	-23.16 ± 0.04	−0.09	$0.50^{+0.92}_{-0.22}$
NGC 4151	SpB	no	20.0	$0.65^{+0.07}_{-0.07}$	$-23.40^{+0.66}_{-0.58}$	-24.44 ± 0.19	−0.09	$2.8^{+4.8}_{-1.5}$
NGC 4261	E	yes	30.8	5^{+1}_{-1}	$-25.72^{+0.66}_{-0.58}$	-25.76 ± 0.20	−0.12	18^{+30}_{-10}
NGC 4291	E	yes	25.5	$3.3^{+0.9}_{-2.5}$	$-24.05^{+0.66}_{-0.58}$	-24.05 ± 0.14	−0.11	$3.9^{+6.7}_{-2.1}$
NGC 4388	SpB	no?	17.0	$0.075^{+0.002}_{-0.002}$	$-21.26^{+0.88}_{-0.66}$	-23.50 ± 0.03 *	−0.07	$0.46^{+0.85}_{-0.21}$
NGC 4459	S0	no	15.7	$0.68^{+0.13}_{-0.13}$	$-23.48^{+0.66}_{-0.58}$	-24.01 ± 0.05	−0.09	$2.9^{+5.0}_{-1.6}$

Galaxy	**Type**	**Core**	**Distance**	$M_{\mathbf{BH}}$	$MAG_{\mathbf{sph}}$	$MAG_{\mathbf{gal}}$	$\mathbf{[3.6]-[4.5]}$	$M_{*,\mathbf{sph}}$
			[Mpc]	[10^8 M$_\odot$]	[mag]	[mag]	[mag]	[10^{10} M$_\odot$]
(1)	(2)	(3)	(4)	(5)	(6)	(7)	(8)	(9)
NGC 4473	E	no	15.3	$1.2^{+0.4}_{-0.9}$	$-23.88^{+0.66}_{-0.58}$	-24.11 ± 0.02	-0.10	$3.9^{+6.6}_{-2.1}$
NGC 4564	S0	no	14.6	$0.60^{+0.03}_{-0.09}$	$-22.30^{+0.18}_{-0.11}$	-22.99 ± 0.07	-0.11	$0.82^{+0.91}_{-0.70}$
NGC 4596	S0B	no	17.0	$0.79^{+0.38}_{-0.33}$	$-22.73^{+0.18}_{-0.11}$	-24.18 ± 0.05	-0.08	$1.6^{+1.7}_{-1.3}$
NGC 4697	E	no	11.4	$1.8^{+0.2}_{-0.1}$	$-24.82^{+0.88}_{-0.66}$	-24.94 ± 0.00	-0.09	10^{+18}_{-4}
NGC 4889	E	yes	103.2	210^{+160}_{-160}	$-27.54^{+0.18}_{-0.11}$	-27.54 ± 0.00	-0.12	91^{+101}_{-77}
NGC 4945	SpB	no?	3.8	$0.014^{+0.014}_{-0.007}$	$-20.96^{+0.66}_{-0.58}$	-23.79 ± 0.22 *	-0.06	$0.36^{+0.62}_{-0.20}$
NGC 5077	E	yes	41.2	$7.4^{+4.7}_{-3.0}$	$-25.45^{+0.18}_{-0.11}$	-25.45 ± 0.06	-0.11	15^{+17}_{-13}
NGC 5128	merger	no?	3.8	$0.45^{+0.17}_{-0.10}$	$-23.89^{+0.88}_{-0.66}$	-24.97 ± 0.13	-0.07	$5.0^{+9.1}_{-2.2}$
NGC 5576	E	no	24.8	$1.6^{+0.3}_{-0.4}$	$-24.44^{+0.18}_{-0.11}$	-24.44 ± 0.07	-0.09	$7.1^{+7.9}_{-6.0}$
NGC 5845	S0	no	25.2	$2.6^{+0.4}_{-1.5}$	$-22.96^{+0.88}_{-0.66}$	-23.10 ± 0.13	-0.12	$1.4^{+2.6}_{-0.6}$
NGC 5846	E	yes	24.2	11^{+1}_{-1}	$-25.81^{+0.66}_{-0.58}$	-25.81 ± 0.10	-0.10	22^{+38}_{-12}
NGC 6251	E	yes?	104.6	5^{+2}_{-2}	$-26.75^{+0.18}_{-0.11}$	-26.75 ± 0.11	-0.12	46^{+51}_{-39}
NGC 7052	E	yes	66.4	$3.7^{+2.6}_{-1.5}$	$-26.32^{+0.18}_{-0.11}$	-26.32 ± 0.03	-0.11	33^{+36}_{-28}
NGC 7619	E	yes	51.5	25^{+8}_{-3}	$-26.35^{+0.66}_{-0.58}$	-26.41 ± 0.16	-0.11	33^{+56}_{-18}
NGC 7768	E	yes	112.8	13^{+5}_{-4}	$-26.90^{+0.66}_{-0.58}$	-26.90 ± 0.02	-0.11	57^{+98}_{-31}
UGC 03789	SpB	no?	48.4	$0.108^{+0.005}_{-0.005}$	$-22.77^{+0.88}_{-0.66}$	-24.20 ± 0.15	-0.07	$1.9^{+3.4}_{-0.8}$

TABLE 2
Linear regression analysis. **X0 is the average X of the subsample...**

Subsample (size)	Regression	α	β	X_0	ϵ	Δ
	Black hole mass – spheroid luminosity $\log[M_{\rm BH}/{\rm M}_\odot] = \alpha + \beta[(MAG_{\rm sph} - X_0)/{\rm mag}]$					
All (66)	BCES OLS($Y\|X$)	8.16 ± 0.07	-0.44 ± 0.04	-23.86	–	0.56
	BCES OLS($X\|Y$)	8.16 ± 0.08	-0.61 ± 0.05	-23.86	–	0.68
	BCES Bisector	8.16 ± 0.07	-0.52 ± 0.04	-23.86	–	0.60
	mFITEXY OLS($Y\|X$)	$8.17^{+0.07}_{-0.06}$	$-0.43^{+0.03}_{-0.03}$	-23.86	$0.49^{+0.06}_{-0.05}$	0.56
	mFITEXY OLS($X\|Y$)	$8.15^{+0.07}_{-0.08}$	$-0.61^{+0.05}_{-0.05}$	-23.86	$0.58^{+0.07}_{-0.06}$	0.67
	mFITEXY Bisector	$8.16^{+0.07}_{-0.07}$	$-0.51^{+0.04}_{-0.04}$	-23.86	–	0.60
	Kelly OLS($Y\|X$)	8.16 ± 0.07	-0.42 ± 0.04	-23.86	0.51 ± 0.06	0.56
	Kelly OLS($X\|Y$)	8.16 ± 0.09	-0.60 ± 0.06	-23.86	0.60 ± 0.09	0.67
	Kelly Bisector	8.16 ± 0.08	-0.51 ± 0.09	-23.86	–	0.59
$n > 2$ (43)	BCES OLS($Y\|X$)	8.58 ± 0.07	-0.42 ± 0.06	-24.77	–	0.46
	BCES OLS($X\|Y$)	8.58 ± 0.08	-0.58 ± 0.06	-24.77	–	0.56
	BCES Bisector	8.58 ± 0.07	-0.50 ± 0.05	-24.77	–	0.49
	mFITEXY OLS($Y\|X$)	$8.57^{+0.07}_{-0.06}$	$-0.41^{+0.04}_{-0.04}$	-24.77	$0.38^{+0.06}_{-0.06}$	0.46
	mFITEXY OLS($X\|Y$)	$8.56^{+0.08}_{-0.08}$	$-0.57^{+0.06}_{-0.07}$	-24.77	$0.44^{+0.08}_{-0.11}$	0.55
	mFITEXY Bisector	$8.57^{+0.07}_{-0.07}$	$-0.49^{+0.05}_{-0.05}$	-24.77	–	0.49
	Kelly OLS($Y\|X$)	8.56 ± 0.07	-0.39 ± 0.05	-24.77	0.40 ± 0.06	0.46
	Kelly OLS($X\|Y$)	8.55 ± 0.09	-0.57 ± 0.08	-24.77	0.49 ± 0.10	0.55
	Kelly Bisector	8.55 ± 0.08	-0.5 ± 0.1	-24.77	–	0.49
Core-Sérsic (22)	BCES OLS($Y\|X$)	9.06 ± 0.09	-0.3 ± 0.1	-25.73	–	0.42
	BCES OLS($X\|Y$)	9.1 ± 0.1	-0.6 ± 0.1	-25.73	–	0.61
	BCES Bisector	9.1 ± 0.1	-0.47 ± 0.08	-25.73	–	0.48
	mFITEXY OLS($Y\|X$)	$9.06^{+0.09}_{-0.08}$	$-0.26^{+0.07}_{-0.08}$	-25.73	$0.37^{+0.08}_{-0.06}$	0.42
	mFITEXY OLS($X\|Y$)	$9.0^{+0.1}_{-0.1}$	$-0.7^{+0.2}_{-0.3}$	-25.73	$0.61^{+0.14}_{-0.09}$	0.67
	mFITEXY Bisector	$9.0^{+0.1}_{-0.1}$	$-0.5^{+0.1}_{-0.2}$	-25.73	–	0.48
	Kelly OLS($Y\|X$)	9.0 ± 0.1	-0.24 ± 0.09	-25.73	0.40 ± 0.08	0.42
	Kelly OLS($X\|Y$)	9.0 ± 0.2	-0.7 ± 0.3	-25.73	0.68 ± 0.30	0.64
	Kelly Bisector	9.0 ± 0.1	-0.4 ± 0.1	-25.73	–	0.46
Sérsic (44)	BCES OLS($Y\|X$)	7.71 ± 0.09	-0.41 ± 0.08	-22.92	–	0.61
	BCES OLS($X\|Y$)	7.7 ± 0.1	-0.9 ± 0.2	-22.92	–	0.93
	BCES Bisector	7.7 ± 0.1	-0.61 ± 0.08	-22.92	–	0.71
	mFITEXY OLS($Y\|X$)	$7.72^{+0.08}_{-0.08}$	$-0.41^{+0.07}_{-0.07}$	-22.92	$0.54^{+0.09}_{-0.07}$	0.61
	mFITEXY OLS($X\|Y$)	$7.7^{+0.1}_{-0.1}$	$-0.9^{+0.1}_{-0.2}$	-22.92	$0.77^{+0.13}_{-0.10}$	0.93
	mFITEXY Bisector	$7.7^{+0.1}_{-0.1}$	$-0.61^{+0.09}_{-0.12}$	-22.92	–	0.71
	Kelly OLS($Y\|X$)	7.73 ± 0.09	-0.41 ± 0.08	-22.92	0.55 ± 0.08	0.61
	Kelly OLS($X\|Y$)	7.7 ± 0.1	-0.9 ± 0.2	-22.92	0.79 ± 0.20	0.93
	Kelly Bisector	7.7 ± 0.1	-0.6 ± 0.1	-22.92	–	0.71
Early-type (E+S0) (45)	BCES OLS($Y\|X$)	8.56 ± 0.07	-0.33 ± 0.04	-24.47	–	0.46
	BCES OLS($X\|Y$)	8.56 ± 0.08	-0.48 ± 0.05	-24.47	–	0.55
	BCES Bisector	$\mathbf{8.56 \pm 0.07}$	$\mathbf{-0.40 \pm 0.04}$	$\mathbf{-24.47}$	–	**0.49**
	mFITEXY OLS($Y\|X$)	$8.56^{+0.06}_{-0.06}$	$-0.32^{+0.03}_{-0.04}$	-24.47	$0.40^{+0.06}_{-0.05}$	0.46
	mFITEXY OLS($X\|Y$)	$8.54^{+0.08}_{-0.08}$	$-0.49^{+0.05}_{-0.06}$	-24.47	$0.49^{+0.08}_{-0.06}$	0.57
	mFITEXY Bisector	$8.55^{+0.07}_{-0.07}$	$-0.41^{+0.04}_{-0.05}$	-24.47	–	0.49
	Kelly OLS($Y\|X$)	8.55 ± 0.07	-0.32 ± 0.04	-24.47	0.41 ± 0.06	0.46
	Kelly OLS($X\|Y$)	8.55 ± 0.09	-0.48 ± 0.06	-24.47	0.51 ± 0.10	0.56
	Kelly Bisector	8.55 ± 0.08	-0.40 ± 0.09	-24.47	–	0.49
Late-type (Sp) (17)	BCES OLS($Y\|X$)	7.2 ± 0.2	-0.8 ± 0.4	-22.33	–	0.70
	BCES OLS($X\|Y$)	7.2 ± 0.3	-1.7 ± 0.7	-22.33	–	1.26
	BCES Bisector	$\mathbf{7.2 \pm 0.2}$	$\mathbf{-1.1 \pm 0.3}$	$\mathbf{-22.33}$	–	**0.88**
	mFITEXY OLS($Y\|X$)	$7.2^{+0.1}_{-0.1}$	$-0.5^{+0.2}_{-0.2}$	-22.33	$0.55^{+0.15}_{-0.10}$	0.62
	mFITEXY OLS($X\|Y$)	$7.4^{+0.5}_{-0.3}$	$-2.0^{+0.7}_{-2.4}$	-22.33	$1.08^{+0.40}_{-0.24}$	1.50
	mFITEXY Bisector	$7.3^{+0.4}_{-0.3}$	$-1.0^{+0.3}_{-0.5}$	-22.33	–	0.82
	Kelly OLS($Y\|X$)	7.2 ± 0.2	-0.5 ± 0.3	-22.33	0.64 ± 0.16	0.62
	Kelly OLS($X\|Y$)	7.3 ± 0.4	-1.9 ± 1.2	-22.33	1.3 ± 0.9	1.4
	Kelly Bisector	7.3 ± 0.3	-0.9 ± 0.5	-22.33	–	0.78

TABLE 3
LINEAR REGRESSION ANALYSIS. **X0 is the average X of the subsample...**

Subsample (size)	**Regression**	$\boldsymbol{\alpha}$	$\boldsymbol{\beta}$	$\boldsymbol{X_0}$	$\boldsymbol{\epsilon}$	$\boldsymbol{\Delta}$
	Black hole mass – galaxy luminosity $\log[M_{\rm BH}/{\rm M}_\odot] = \alpha + \beta[(MAG_{\rm gal} - X_0)/{\rm mag}]$					
All (62)	BCES OLS($Y\|X$)	8.26 ± 0.08	-0.49 ± 0.06	-24.78	–	0.64
	BCES OLS($X\|Y$)	8.3 ± 0.1	-1.0 ± 0.1	-24.78	–	0.92
	BCES Bisector	8.26 ± 0.09	-0.72 ± 0.07	-24.78	–	0.71
	mFITEXY OLS($Y\|X$)	$8.26^{+0.08}_{-0.08}$	$-0.49^{+0.06}_{-0.07}$	-24.78	$0.61^{+0.07}_{-0.05}$	0.64
	mFITEXY OLS($X\|Y$)	$8.3^{+0.1}_{-0.1}$	$-1.0^{+0.1}_{-0.2}$	-24.78	$0.88^{+0.10}_{-0.08}$	0.93
	mFITEXY Bisector	$8.3^{+0.1}_{-0.1}$	$-0.72^{+0.09}_{-0.10}$	-24.78	–	0.71
	Kelly OLS($Y\|X$)	8.26 ± 0.08	-0.49 ± 0.07	-24.78	0.63 ± 0.07	0.64
	Kelly OLS($X\|Y$)	8.3 ± 0.1	-1.0 ± 0.1	-24.78	0.91 ± 0.17	0.93
	Kelly Bisector	8.3 ± 0.1	-0.7 ± 0.1	-24.78	–	0.71
Early-type (E+S0) (45)	BCES OLS($Y\|X$)	8.56 ± 0.06	-0.43 ± 0.05	-24.88	–	0.45
	BCES OLS($X\|Y$)	8.56 ± 0.08	-0.63 ± 0.05	-24.88	–	0.53
	BCES Bisector	8.56 ± 0.07	-0.53 ± 0.04	-24.88	–	0.47
	mFITEXY OLS($Y\|X$)	$8.56^{+0.06}_{-0.06}$	$-0.42^{+0.05}_{-0.05}$	-24.88	$0.41^{+0.06}_{-0.05}$	0.45
	mFITEXY OLS($X\|Y$)	$8.56^{+0.08}_{-0.08}$	$-0.66^{+0.06}_{-0.08}$	-24.88	$0.51^{+0.07}_{-0.06}$	0.55
	mFITEXY Bisector	$8.56^{+0.07}_{-0.07}$	$-0.54^{+0.06}_{-0.06}$	-24.88	–	0.47
	Kelly OLS($Y\|X$)	8.56 ± 0.07	-0.42 ± 0.06	-24.88	0.43 ± 0.06	0.45
	Kelly OLS($X\|Y$)	8.56 ± 0.09	-0.65 ± 0.08	-24.88	0.53 ± 0.10	0.54
	Kelly Bisector	8.56 ± 0.08	-0.5 ± 0.1	-24.88	–	0.47
	Black hole mass – spheroid stellar mass $\log[M_{\rm BH}/{\rm M}_\odot] = \alpha + \beta \log[(M_{*,\rm sph} - X_0)/{\rm M}_\odot]$					
Early-type (E+S0) (45)	BCES OLS($Y\|X$)	8.56 ± 0.07	0.8 ± 0.1	10.81	–	0.48
	BCES OLS($X\|Y$)	8.56 ± 0.08	1.3 ± 0.1	10.81	–	0.59
	BCES Bisector	$\mathbf{8.56 \pm 0.07}$	$\mathbf{1.0 \pm 0.1}$	**10.81**	–	**0.51**
	mFITEXY OLS($Y\|X$)	$8.56^{+0.06}_{-0.07}$	$0.8^{+0.1}_{-0.1}$	10.81	$0.42^{+0.06}_{-0.05}$	0.48
	mFITEXY OLS($X\|Y$)	$8.54^{+0.09}_{-0.08}$	$1.3^{+0.2}_{-0.1}$	10.81	$0.53^{+0.08}_{-0.07}$	0.61
	mFITEXY Bisector	$8.55^{+0.07}_{-0.08}$	$1.0^{+0.1}_{-0.1}$	10.81	–	0.51
	Kelly OLS($Y\|X$)	8.55 ± 0.07	0.8 ± 0.1	10.81	0.43 ± 0.06	0.48
	Kelly OLS($X\|Y$)	8.55 ± 0.09	1.3 ± 0.2	10.81	0.54 ± 0.11	0.59
	Kelly Bisector	8.55 ± 0.08	1.0 ± 0.2	10.81	–	0.51
Late-type (Sp) (17)	BCES OLS($Y\|X$)	7.2 ± 0.2	1.9 ± 1.5	10.05	–	0.74
	BCES OLS($X\|Y$)	7.2 ± 0.4	5.9 ± 3.4	10.05	–	1.70
	BCES Bisector	$\mathbf{7.2 \pm 0.2}$	$\mathbf{3.0 \pm 1.3}$	**10.05**	–	**0.94**
	mFITEXY OLS($Y\|X$)	$7.2^{+0.1}_{-0.2}$	$1.2^{+0.7}_{-0.6}$	10.05	$0.59^{+0.16}_{-0.11}$	0.66
	mFITEXY OLS($X\|Y$)	$7.4^{+1.5}_{-0.5}$	$7.1^{+26.3}_{-3.0}$	10.05	$1.49^{+0.57}_{-0.35}$	2.08
	mFITEXY Bisector	$7.2^{+1.0}_{-0.4}$	$2.3^{+1.7}_{-1.0}$	10.05	–	0.79
	Kelly OLS($Y\|X$)	7.2 ± 0.2	0.9 ± 0.9	10.05	0.67 ± 0.16	0.65
	Kelly OLS($X\|Y$)	7.4 ± 0.6	7.0 ± 6.6	10.05	1.83 ± 1.82	2.04
	Kelly Bisector	7.3 ± 0.5	1.9 ± 203.0	10.05	–	0.74

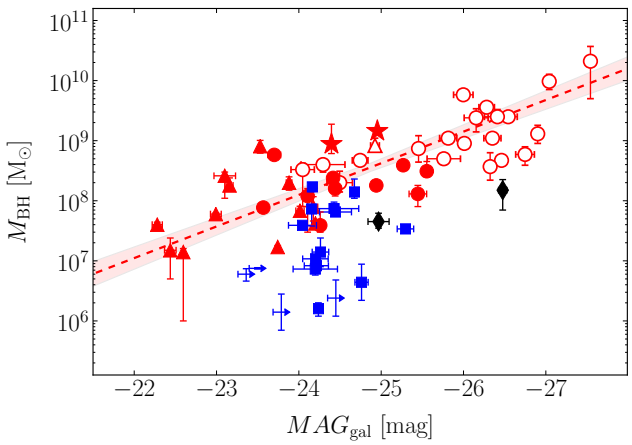

FIG. 3.— Black hole mass against 3.6 μm galaxy absolute magnitude. Symbols are coded as in Figure 1. Four spiral galaxies had their magnitudes overestimated and are shown as upper limits.

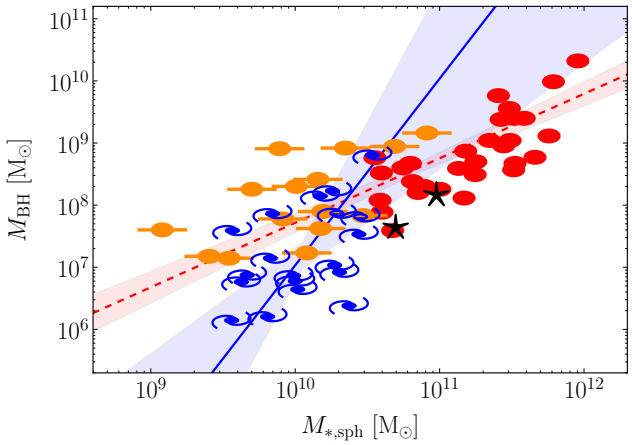

FIG. 4.— Black hole mass against spheroid stellar mass. Symbols are coded according to the galaxy morphological type (red = E, orange = E/S0 and S0, blue = S0/Sp and Sp, black = merger). The red dashed line indicates the BCES bisector linear regression for early-type galaxies (ellipticals+lenticulars), with the red shaded area denoting its 1σ uncertainty. The blue solid line shows the BCES bisector linear regression for spiral galaxies, with the blue shaded area denoting its 1σ uncertainty.

to quantify it. In Table 3, we report the BCES, modified FITEXY and `linmix_err` linear regressions, both symmetrical and non-symmetrical, for Sérsic/core-Sérsic galaxies and for different galaxy morphological types (elliptical/lenticular, spiral). Symmetrical regressions are meant to be compared with theoretical expectations, whereas non-symmetrical Ordinary Least Squares ($Y|X$) regressions – since they minimize the scatter in the vertical direction – can be used to predict black hole masses.

4. RESULTS AND DISCUSSION

4.1. *Black hole mass – spheroid luminosity*

We show the $M_{\rm BH} - L_{\rm sph}$ diagram in Figure 1. Sérsic and core-Sérsic spheroids have slopes consistent with each other (within their 1σ uncertainties), in disagreement with the findings of GS13. The slope that we obtained for core-Sérsic spheroids ($M_{\rm BH} \propto L_{\rm sph}^{1.2\pm0.2}$) is consistent with the slope reported by GS13 in the K_s-band ($M_{\rm BH} \propto L_{\rm sph}^{1.1\pm0.2}$). Instead, the slope that we determined for Sérsic spheroids ($M_{\rm BH} \propto L_{\rm sph}^{1.5\pm0.2}$) is significantly shallower than that found by GS13 ($M_{\rm BH} \propto L_{\rm sph}^{2.7\pm0.5}$). Although the Sérsic/core-Sérsic classification used by GS13 slightly differs[7] from the classification used here, the main cause of such inconsistency is that the bulge-to-total ratios obtained from our galaxy decompositions are different from those assumed by GS13 to convert galaxy luminosities into bulge luminosities. Our bulge-to-total ratios for low-luminosity Sérsic spheroids ($MAG_{\rm sph} \gtrsim -22$ mag) are smaller than those used by GS13. The host galaxies of such bulges are late-type, spiral galaxies, which typically present a complex morphology (bars, double bars, embedded disks, nuclear components, etc). Our sophisticated galaxy models account for the extra components, while the bulge-to-total ratios of GS13 were derived from simple bulge/disk decompositions which overestimated the bulge luminosity. This results in our bulge magnitudes being on average ∼1 mag fainter. On the other side, our bulge-to-total ratios for high-luminosity Sérsic spheroids ($MAG_{\rm sph} \lesssim -24$ mag) are on average larger than those adopted by GS13. In this case, the host systems are early-type elliptical/lenticular galaxies that feature intermediate-scale disks[8]. Past bulge/disk decompositions failed to correctly identify the extent of such disks and treated them as large-scale disks, thus underestimating the bulge luminosity. The magnitudes that we obtained for such spheroids are on average ∼1 mag brighter.

We have seen that the change in slope of the $M_{\rm BH} - L_{\rm sph}$ correlation – which is expected for consistency with other scaling relations (a single power-law $M_{\rm BH} - \sigma$ correlation and a double power-law $L_{\rm sph} - \sigma$ correlation) – cannot be attributed to the division between the two populations of Sérsic and core-Sérsic spheroids. We now test a new hypothesis, that is to say the change in slope is to be ascribed to the different formation mechanisms of early- and late-type galaxies. If this hypothesis is correct, the spheroids of early-type (elliptical and lenticular) galaxies will follow $M_{\rm BH} \propto L_{\rm sph}^{\sim1}$, whereas the spheroids of late-type (spiral) galaxies will have $M_{\rm BH} \propto L_{\rm sph}^{\sim2.5}$. First, we checked that elliptical and lenticular galaxies, taken separately, have slopes consistent with each other, and thus, taken together, they define a single *red sequence* in the $M_{\rm BH} - L_{\rm sph}$ diagram. We then fit the bulges of early- and late-type galaxies with two separate log-linear regressions, and obtained $M_{\rm BH} \propto L_{\rm sph}^{1\pm0.1}$ and $M_{\rm BH} \propto L_{\rm sph}^{2.75\pm0.75}$ respectively, in excellent agreement with the theoretical expectations of our hypothesis. **AL, can you pls write this: Remember also Ewan's remark about the unsuitability of the Pearson and Spearman correlation coefficients because they do not take into account the error bars on our data - so don't include those simple coefficients. Actually, it would be worth pointing out to readers that a visual inspection of the plotted data re-**

[7] which galaxies?
[8] explain

quires the viewer to take into account the error bars when judging-by-eye the strength of a correlation. Maybe then mention in the following sentence that this is why the correlation coefficients are not applicable here.

4.2. *Pseudo- versus classical bulges*

Current views distinguish between classical bulges, which are considered to be spheroidal, pressure-supported systems, formed through violent processes, such as hierarchical clustering via minor mergers, and pseudo-bulges, thought to be disk-like, rotation-supported systems, built from secular evolution processes, such as instabilities of their surrounding disk or bar. Pseudo-bulges are notoriously hard to identify (Graham 2013, 2014, 2015a,c). For example, mergers can create bulges that rotate (e.g. Bekki 2010; Keselman & Nusser 2012), and bars can spin-up classical bulges (e.g. Saha et al. 2012), thus rotation is not a definitive signature of a pseudobulge. Furthermore, many galaxies host both a pseudo- and a classical bulge (e.g. Erwin et al. 2003, 2015; Athanassoula 2005; Gadotti 2009; MacArthur et al. 2009; dos Anjos & da Silva 2013; Seidel et al. 2015). In the recent literature, pseudo- and classical bulges have been frequently told apart by means of a divide at a Sérsic index of $n_{\rm sph} = 2$ (e.g. Fisher & Drory 2010), although, from a selection of hundreds of disc galaxies imaged in the K-band, Graham & Worley (2008) observed no such bimodality in the bulge Sérsic indices. While pseudo-bulges are expected to have exponential-like surface brightness profiles ($n_{\rm sph} \simeq 1$), being disky components that formed from their surrounding exponential disks (e.g. Bardeen 1975; Hohl 1975; Combes & Sanders 1981; Combes et al. 1990; Pfenniger & Friedli 1991), it has been shown that mergers can create bulges with $n_{\rm sph} < 2$ (e.g. Eliche-Moral et al. 2011; Scannapieco et al. 2011; Querejeta et al. 2015), just as low-luminosity elliptical galaxies (not built from the secular evolution of a disk) are well known to have $n_{\rm sph} < 2$ and even $n_{\rm sph} < 1$ (e.g. Davies et al. 1988; Young & Currie 1994). Sani et al. (2011) reported that pseudo-bulges – which they labelled as such according to the $n_{\rm sph} < 2$ criterion – with low black hole masses ($M_{\rm BH} < 10^7$ M$_\odot$) are significantly displaced from the correlation traced by classical bulges. In Figure 2, we show the distribution of spheroid Sérsic indices[9] in the $M_{\rm BH} - L_{\rm sph}$ diagram. Our aim is to check whether $n_{\rm sph} < 2$ bulges are offset to lower black hole masses from the correlation defined by $n_{\rm sph} > 2$ bulges. To do this, we fit a symmetrical linear regression to the bulges that have $n_{\rm sph} > 2$ and we compute the vertical offset of all bulges from the regression. In the inset of Figure 2, we plot the vertical offset against $n_{\rm sph}$. From a visual inspection, bulges with $n_{\rm sph} < 2$ do not appear to be offset from the correlation traced by bulges with $n_{\rm sph} > 2$.

4.3. *Black hole mass – galaxy luminosity*

Figure 3 illustrates the $M_{\rm BH} - L_{\rm gal}$ diagram. Four spiral galaxies had their total luminosities underestimated (see Section 2) and thus are not included in the linear regression analysis.

Upon analyzing a sample of 35 galaxies, among which only four were classified as spiral galaxies, Läsker et al. (2014b) claimed that the $M_{\rm BH} - L_{\rm sph}$ and $M_{\rm BH} - L_{\rm gal}$ relations, which they fit with a single power-law, have consistent intrinsic scatter. Here, instead, thanks to our double-sized galaxy sample that includes 17 spiral galaxies, we show that the claim made by Läsker et al. (2014b) is valid only for early-type galaxies. The $M_{\rm BH} - L_{\rm sph}$ correlation for all galaxies, irrespective of their morphological type, has intrinsic scatter $\epsilon_{(Y|X)} = 0.51 \pm 0.06$ dex (direct linear regression) and $\epsilon_{(X|Y)} = 0.60 \pm 0.09$ dex (inverse linear regression), whereas the $M_{\rm BH} - L_{\rm gal}$ correlation for all galaxies has $\epsilon_{(Y|X)} = 0.63 \pm 0.07$ dex and $\epsilon_{(X|Y)} = 0.91 \pm 0.17$ dex. However, when considering only early-type galaxies, we find that the $M_{\rm BH} - L_{\rm sph}$ and $M_{\rm BH} - L_{\rm gal}$ relations have the same level of intrinsic scatter. Because the value of the intrinsic scatter depends on the uncertainties associated to the luminosities[10], we tested the robustness of our last conclusion by increasing/decreasing the errors associated to $L_{\rm gal}$ (that we originally assumed to be 0.25 mag) and repeating the linear regression analysis. On the other hand, the uncertainties associated to $L_{\rm sph}$ have been estimated with an advanced method that takes into account the systematic errors related to the galaxy decomposition process. We consider these uncertainties trustworthy and, therefore, we decided to vary only the errors associated to $L_{\rm gal}$. We found that the $M_{\rm BH} - L_{\rm sph}$ and $M_{\rm BH} - L_{\rm gal}$ relations for early-type galaxies have inconsistent intrinsic scatter when assuming an error ≥ 0.7 mag on $L_{\rm gal}$. Because such error is larger than the typical error on $L_{\rm sph}$ used here – and, in general, is significantly larger than the uncertainties on $L_{\rm gal}$ that are typically used in the literature –, we come to the conclusion that our determination of the intrinsic scatter is reliable, and that, for early-type galaxies, $M_{\rm BH}$ correlates equally well with $L_{\rm sph}$ and $L_{\rm gal}$. As Läsker et al. (2014b) pointed out, from the observer's perspective, measuring galaxy luminosities is obviously easier and faster than performing accurate galaxy decompositions to obtain bulge luminosities. This, combined with our last conclusion, suggests that one should prefer the galaxy luminosity over the bulge luminosity to predict black hole masses when dealing with samples of elliptical and lenticular galaxies only.

4.4. *Black hole mass – spheroid stellar mass*

Finally, we present the $M_{\rm BH} - M_{*,\rm sph}$ diagram in Figure 4.

relations agns consistent w spirals, but analysis deferred to other paper cubic growth

5. CONCLUSIONS

ngc0524 outlier, n1332 non outlier

GS warmly thanks Luca Cortese, Elisabete Lima Da Cunha and Gonzalo Diaz for useful discussion.
This research was supported by Australian Research Council funding through grants DP110103509 and FT110100263. This work is based on observations made

[9] The spheroid Sérsic indices are taken from our one-dimensional fits of the galaxy major-axis surface brightness profiles (*Paper I*).

[10] The smaller (larger) the uncertainties, the larger (smaller) the intrinsic scatter.

with the IRAC instrument (Fazio et al. 2004) on-board the Spitzer Space Telescope, which is operated by the Jet Propulsion Laboratory, California Institute of Technology under a contract with NASA. This research has made use of the GOLDMine database (Gavazzi et al. 2003) and the NASA/IPAC Extragalactic Database (NED) which is operated by the Jet Propulsion Laboratory, California Institute of Technology, under contract with the National Aeronautics and Space Administration. The BCES routine (Akritas & Bershady 1996) was run via the python module written by Rodrigo Nemmen (Nemmen et al. 2012), which is available at https://github.com/rsnemmen/BCES.

REFERENCES

Akritas, M. G., & Bershady, M. A. 1996, ApJ, 470, 706
Arnold, J. A., Romanowsky, A. J., Brodie, J. P., et al. 2014, ApJ, 791, 80
Athanassoula, E. 2005, MNRAS, 358, 1477
Balcells, M., Graham, A. W., & Peletier, R. F. 2007, ApJ, 665, 1104
Bardeen, J. M. 1975, in IAU Symposium, Vol. 69, Dynamics of the Solar Systems, ed. A. Hayli, 297
Beifiori, A., Courteau, S., Corsini, E. M., & Zhu, Y. 2012, MNRAS, 419, 2497
Bekki, K. 2010, MNRAS, 401, L58
Chilingarian, I. V., Cayatte, V., Durret, F., et al. 2008, A&A, 486, 85
Cody, A. M., Carter, D., Bridges, T. J., Mobasher, B., & Poggianti, B. M. 2009, MNRAS, 396, 1647
Combes, F., Debbasch, F., Friedli, D., & Pfenniger, D. 1990, A&A, 233, 82
Combes, F., & Sanders, R. H. 1981, A&A, 96, 164
Davies, J. I., Phillipps, S., Cawson, M. G. M., Disney, M. J., & Kibblewhite, E. J. 1988, MNRAS, 232, 239
Davies, R. L., Efstathiou, G., Fall, S. M., Illingworth, G., & Schechter, P. L. 1983, ApJ, 266, 41
de Rijcke, S., Michielsen, D., Dejonghe, H., Zeilinger, W. W., & Hau, G. K. T. 2005, A&A, 438, 491
dos Anjos, S., & da Silva, M. B. 2013, Memorie della Societa Astronomica Italiana Supplementi, 25, 33
Dressler, A. 1989, in IAU Symposium, Vol. 134, Active Galactic Nuclei, ed. D. E. Osterbrock & J. S. Miller, 217
Dullo, B. T., & Graham, A. W. 2014, MNRAS, 444, 2700
Eliche-Moral, M. C., González-García, A. C., Balcells, M., et al. 2011, A&A, 533, A104
Emsellem, , & E. et al. 2011, MNRAS, 414, 888
Erwin, P., Beltrán, J. C. V., Graham, A. W., & Beckman, J. E. 2003, ApJ, 597, 929
Erwin, P., & Gadotti, D. A. 2012, Advances in Astronomy, 2012, 4
Erwin, P., Saglia, R., Thomas, J., et al. 2015, in IAU Symposium, Vol. 309, IAU Symposium, ed. B. L. Ziegler, F. Combes, H. Dannerbauer, & M. Verdugo, 359–360
Fazio, G. G., Hora, J. L., Allen, L. E., et al. 2004, ApJS, 154, 10
Ferrarese, L., & Ford, H. 2005, Space Sci. Rev., 116, 523
Ferrarese, L., & Merritt, D. 2000, ApJ, 539, L9
Fisher, D. B., & Drory, N. 2010, ApJ, 716, 942
Forbes, D. A., Lasky, P., Graham, A. W., & Spitler, L. 2008, MNRAS, 389, 1924
Gadotti, D. A. 2009, MNRAS, 393, 1531
Gavazzi, G., Boselli, A., Donati, A., Franzetti, P., & Scodeggio, M. 2003, A&A, 400, 451
Gebhardt, K., Bender, R., Bower, G., et al. 2000, ApJ, 539, L13
Graham, A. 2015a, Highlights of Astronomy, 16, 360
Graham, A. W. 2007, MNRAS, 379, 711
—. 2008, PASA, 25, 167
—. 2012, ApJ, 746, 113
—. 2013, Elliptical and Disk Galaxy Structure and Modern Scaling Laws, ed. T. D. Oswalt & W. C. Keel, 91
Graham, A. W. 2014, in Astronomical Society of the Pacific Conference Series, Vol. 480, Structure and Dynamics of Disk Galaxies, ed. M. S. Seigar & P. Treuthardt, 185
—. 2015b, ArXiv e-prints, arXiv:1501.02937
—. 2015c, ArXiv e-prints, arXiv:1501.02937
Graham, A. W., Erwin, P., Trujillo, I., & Asensio Ramos, A. 2003, AJ, 125, 2951
Graham, A. W., & Guzmán, R. 2003, AJ, 125, 2936
Graham, A. W., Onken, C. A., Athanassoula, E., & Combes, F. 2011, MNRAS, 412, 2211
Graham, A. W., & Scott, N. 2013, ApJ, 764, 151
—. 2015, ApJ, 798, 54
Graham, A. W., & Worley, C. C. 2008, MNRAS, 388, 1708
Gültekin, K., Richstone, D. O., Gebhardt, K., et al. 2009, ApJ, 698, 198
Häring, N., & Rix, H.-W. 2004, ApJ, 604, L89
Held, E. V., de Zeeuw, T., Mould, J., & Picard, A. 1992, in IAU Symposium, Vol. 149, The Stellar Populations of Galaxies, ed. B. Barbuy & A. Renzini, 429
Hohl, F. 1975, in IAU Symposium, Vol. 69, Dynamics of the Solar Systems, ed. A. Hayli, 349
Jiang, N., Ho, L. C., Dong, X.-B., Yang, H., & Wang, J. 2013, ApJ, 770, 3
Jiang, Y.-F., Greene, J. E., & Ho, L. C. 2011, ApJ, 737, L45
Kelly, B. C. 2007, ApJ, 665, 1489
Keselman, J. A., & Nusser, A. 2012, MNRAS, 424, 1232
Kormendy, J., & Ho, L. C. 2013, ARA&A, 51, 511
Kormendy, J., & Richstone, D. 1995, ARA&A, 33, 581
Kourkchi, E., Khosroshahi, H. G., Carter, D., et al. 2012, MNRAS, 420, 2819
Laor, A. 1998, ApJ, 505, L83
—. 2001, ApJ, 553, 677
Läsker, R., Ferrarese, L., & van de Ven, G. 2014a, ApJ, 780, 69
Läsker, R., Ferrarese, L., van de Ven, G., & Shankar, F. 2014b, ApJ, 780, 70
Lauer, T. R., Faber, S. M., Richstone, D., et al. 2007a, ApJ, 662, 808
—. 2007b, ApJ, 662, 808
Liu, F. S., Xia, X. Y., Mao, S., Wu, H., & Deng, Z. G. 2008, MNRAS, 385, 23
MacArthur, L. A., González, J. J., & Courteau, S. 2009, MNRAS, 395, 28
Magorrian, J., Tremaine, S., Richstone, D., et al. 1998, AJ, 115, 2285
Malumuth, E. M., & Kirshner, R. P. 1981, ApJ, 251, 508
Marconi, A., & Hunt, L. K. 2003, ApJ, 589, L21
Mathur, S., Fields, D., Peterson, B. M., & Grupe, D. 2012, ApJ, 754, 146
Matković, A., & Guzmán, R. 2005, MNRAS, 362, 289
McConnell, N. J., & Ma, C.-P. 2013, ApJ, 764, 184
McConnell, N. J., Ma, C.-P., Gebhardt, K., et al. 2011, Nature, 480, 215
Meidt, S. E., Schinnerer, E., van de Ven, G., et al. 2014, ApJ, 788, 144
Nemmen, R. S., Georganopoulos, M., Guiriec, S., et al. 2012, Science, 338, 1445
Peletier, R. F., Kutdemir, E., van der Wolk, G., et al. 2012, MNRAS, 419, 2031
Pfenniger, D., & Friedli, D. 1991, A&A, 252, 75
Press, W. H., Teukolsky, S. A., Vetterling, W. T., & Flannery, B. P. 1992, Numerical recipes in FORTRAN. The art of scientific computing
Querejeta, M., Eliche-Moral, M. C., Tapia, T., et al. 2015, A&A, 573, A78
Reines, A. E., Greene, J. E., & Geha, M. 2013, ApJ, 775, 116
Rusli, S. P., Erwin, P., Saglia, R. P., et al. 2013a, AJ, 146, 160
Rusli, S. P., Thomas, J., Saglia, R. P., et al. 2013b, AJ, 146, 45
Ryan, C. J., De Robertis, M. M., Virani, S., Laor, A., & Dawson, P. C. 2007, ApJ, 654, 799
Saha, K., Martinez-Valpuesta, I., & Gerhard, O. 2012, MNRAS, 421, 333
Sani, E., Marconi, A., Hunt, L. K., & Risaliti, G. 2011, MNRAS, 413, 1479
Savorgnan, G. A. D., & Graham, A. W. 2014, ArXiv e-prints, arXiv:1410.7405
Scannapieco, C., White, S. D. M., Springel, V., & Tissera, P. B. 2011, MNRAS, 417, 154
Schechter, P. L. 1980, AJ, 85, 801

Scott, N., Davies, R. L., Houghton, R. C. W., et al. 2014, MNRAS, 441, 274
Scott, N., Graham, A. W., & Schombert, J. 2013, ApJ, 768, 76
Seidel, M. K., Cacho, R., Ruiz-Lara, T., et al. 2015, MNRAS, 446, 2837
Sheth, K., Regan, M., Hinz, J. L., et al. 2010, PASP, 122, 1397
Tortora, C., Napolitano, N. R., Romanowsky, A. J., Capaccioli, M., & Covone, G. 2009, MNRAS, 396, 1132
Tremaine, S., Gebhardt, K., Bender, R., et al. 2002, ApJ, 574, 740
Trujillo, I., Erwin, P., Asensio Ramos, A., & Graham, A. W. 2004, AJ, 127, 1917
van den Bosch, R. C. E., Gebhardt, K., Gültekin, K., et al. 2012, Nature, 491, 729
Vika, M., Driver, S. P., Cameron, E., Kelvin, L., & Robotham, A. 2012, MNRAS, 419, 2264
von der Linden, A., Best, P. N., Kauffmann, G., & White, S. D. M. 2007, MNRAS, 379, 867
Wandel, A. 1999, ApJ, 519, L39
Yee, H. K. C. 1992, in Astronomical Society of the Pacific Conference Series, Vol. 31, Relationships Between Active Galactic Nuclei and Starburst Galaxies, ed. A. V. Filippenko, 417
Young, C. K., & Currie, M. J. 1994, MNRAS, 268, L11